Hindawi
Advances in Materials Science and Engineering
Volume 2018, Article ID 5810180, 10 pages
https://doi.org/10.1155/2018/5810180

Research Article

Strength and Failure Mechanism of Composite-Steel Adhesive Bond Single Lap Joints

Kai Wei, Yiwei Chen, Maojun Li, and Xujing Yang

State Key Laboratory of Advanced Design and Manufacturing for Vehicle Body, Hunan University, Changsha, Hunan 410082, China

Correspondence should be addressed to Xujing Yang; yangxujing@hnu.edu.cn

Received 19 October 2017; Accepted 16 January 2018; Published 21 March 2018

Academic Editor: Aniello Riccio

Carbon fiber-reinforced plastics- (CFRP-) steel single lap joints with regard to tensile loading with two levels of adhesives and four levels of overlap lengths were experimentally analyzed and numerically simulated. Both joint strength and failure mechanism were found to be highly dependent on adhesive type and overlap length. Joints with 7779 structural adhesive were more ductile and produced about 2-3 kN higher failure load than MA830 structural adhesive. Failure load with the two adhesives increased about 147 N and 176 N, respectively, with increasing 1 mm of the overlap length. Cohesion failure was observed in both types of adhesive joints. As the overlap length increased, interface failure appeared solely on the edge of the overlap in 7779 adhesive joints. Finite element analysis (FEA) results revealed that peel and shear stress distributions were nonuniform, which were less severe as overlap length increased. Severe stress concentration was observed on the overlap edge, and shear failure of the adhesive was the main reason for the adhesive failure.

1. Introduction

With the aim to save energy and reduce emission, weight saving is of significant importance in the transportation industry. Composite, which exhibits high stiffness-to-weight and strength-to-weight ratios than traditional metal counterparts, has gained widespread usage for lightweight structures. In practical application, it is almost impossible to manufacture a structure as a whole body. Many structures are manufactured as single parts, and then connected through joints. The commonly used methods for joining composite parts are either through mechanical fastening or bonding. Mechanical fasteners including bolts, rivets, and pins have been commonly used for several decades [1–3]. The ease of disassembling components and allowing for reliable inspection has been a great benefit. However, the key problem is that high stress concentrations can develop around the fastener holes, and the joint can be brought to failure at far lower stress levels than expected [4]. Due to its larger bond area to distribute loads and eliminate stress concentration as well as keeping structure integrity, adhesive bonding is more attractive as compared to mechanical fastening joining methods [5].

Extensive researches have been conducted to investigate the bonded joints through analytical, experimental, and numerical methods. Previous researches focused on different affecting factors on the joint strength and damage mechanism [6–10]. The failure load is found to increase with overlap length and adhesive thickness. Material properties and geometry size have been investigated to significantly affect the joint strength and failure modes. On account of the effect of factors mentioned above, researchers latterly focused on improving the strength of the joints. The joint strength increased by modifying the shape of the joint [11, 12] and adding chamfer [13] and fillets [14]. The quality of the bonded joints depends highly on the manufacturing process. Some researchers thus presented surface treatment [15, 16] on the overlap region and curing conditions such as pressure and temperature. For the purpose of optimizing and designing a high-quality joint, stress distributions over the adhesive layer were obtained through numerical methods [17–19]. These simulation works can also predict the joint strength compared to experimental results. Later the finite element method coupled with the cohesive zone model was performed for failure evolution analysis [20, 21]. This can be used to

model the failure initiation and further propagation. Although the mechanical behaviors of the adhesive joints have been investigated as mentioned above, the understanding the strength and failure mechanism of the joints is still local and rough due to the complexity of the mechanical behaviors, especially for joints with composite substrates [22]. Therefore, it is necessary to conduct a detailed research for the CFRP-to-steel adhesive joints.

The present study mainly focused on the mechanical properties and failure behavior of CFRP-to-steel adhesively bonded single lap joints. Different joints were fabricated and tested according to eight different variances, including two kinds of adhesives and four overlap lengths. Mechanical properties were firstly shown and compared with each other. Both the experimental and numerical results about joint strength were then displayed for further detailed analysis. Finite element analysis was then conducted to compare with the experimental results. A detailed stress distribution analysis for various overlap length values was then exhibited, followed by a stress distribution comparison at three typical moments during the tensile process. Failure propagation analysis was carried out for a detailed understanding of the joints' damage evolution. Finally, photographs of the failure joints were exhibited for failure mode analysis.

2. Experiments

2.1. Materials. Two different structural adhesives were used in this study. Type 1 is 7779 adhesive which belongs to two-component polyurethane structural adhesive produced by Ashland. Type 2 (MA830) is a kind of two-liquid acrylic structural adhesive provided by Plexus. Both structural adhesives were prepared and tested to compare the mechanical properties with each other. In this study, the uniaxial tensile test was conducted based on the ISO standard 527-2, which is the determination of tensile properties of plastics. T-peel test was employed with regard to the ISO standard 11339, which is mainly applied for flexible-to-flexible bonded assemblies. And the thick-adherend testing method based on the ISO standard 11003-2 is employed to determine the shear behavior for both structural adhesives. The mechanical properties are finally summarized in Table 1.

The adherends selected for this study were carbon fiber-reinforced plastic (CFRP) laminates and DC04 steel commonly used for automobiles. The CFRP laminates were prepared using the vacuum-assisted resin infusion molding process. Carbon fiber (CC-P400-12) was employed as the reinforcement, and weft and warp were balanced plain woven. Each ply has a thickness of 0.44 mm, and 4 plies were used with 0°/90° ply orientation. The epoxy (MA-8931A/B) was selected as the matrix. When the carbon fiber was soaked with resin under the impact of atmospheric pressure, the whole specimen was moved to a heating oven for curing at 120°C for 6 minutes. The whole specimen was then released from the mould after being cured and cut into the required size. The mechanical properties of the CFRP are listed in Table 2. Another selected adherend is DC04 steel, which is a kind of deep drawing steel with low yield strength and high ductility. It is widely used in the complex parts of automobile. The mechanical properties of the DC04 steel are listed in Table 3.

Table 1: Mechanical properties of the two adhesives.

Mechanical properties	7779	MA830
Young's modulus, E (MPa)	1169	665
Tensile strength, σ (MPa)	29.43	25.06
Shear modulus, G (MPa)	389	251
Shear strength, τ (MPa)	20.40	18.49
Facture energy release rate in tension, G_T (N/mm)	2.75	0.56
Facture energy release rate in shear, G_S (N/mm)	2.03	1.23

Table 2: Mechanical properties of the CFRP adherend.

Mechanical properties	Value	Mechanical properties	Value
$E1$ (MPa)	26580	σ_1 (MPa)	883
$E2$ (MPa)	26580	σ_2 (MPa)	883
$E3$ (MPa)	3880	σ_3 (MPa)	87
$G12$ (MPa)	8482	$V12$	0.35
$G13$ (MPa)	3678	$V13$	0.3
$G23$ (MPa)	3678	$V23$	0.3

2.2. Single Lap Joints. The geometry size of the single lap joint for tensile testing according to ISO 4587 is presented in Figure 1. The various overlap length with regard to the experiment requirement between the CFRP laminate and DC04 substrate is denoted as L_0. L represents the whole length of the specimen. The compensating plate was prepared with the same thickness corresponding to specific adherend.

According to literature review [14], the abrasive paper of grit size up to 1000 was used to polish the substrates, and acetone was applied to eliminate impurity of the substrate surfaces. Compensating plates were firstly bonded to the corresponding adherends, and lines in both adherends were drawn to dominate the overlap length. Adhesive was then evenly distributed on the overlap region of the DC04 substrates. Four small steel wires were employed to control the adhesive thickness in this process. The two substrates were boned together using a clip, and the whole specimen was finally put into an oven to cure for 2.5 h under the temperature of 80°C.

A full-factorial experimental design was employed with two levels of adhesive and four levels of overlap length giving total number of 8 tests. The detailed experiment with corresponding factors and levels is listed in Table 4. A quasistatic loading with the velocity of 2 mm/min was applied in tensile testing. For improving experimental accuracy, three replicates were conducted for each trial, and the normalized peak loads and failure displacements were recorded.

3. Finite Element Analysis

A numerical model was implemented and developed using the commercial software ABAQUS. The objective of finite element analysis (FEA) is to develop a model that could accurately predict the experimental results and present a detailed

Table 3: Mechanical properties of the DC04 adherend.

Adherend material	Young modulus (GPa)	Tensile strength (MPa)	Yield strength (MPa)	Elongation ratio	Poisson's ratio
DC04	203	316	170	78%	0.31

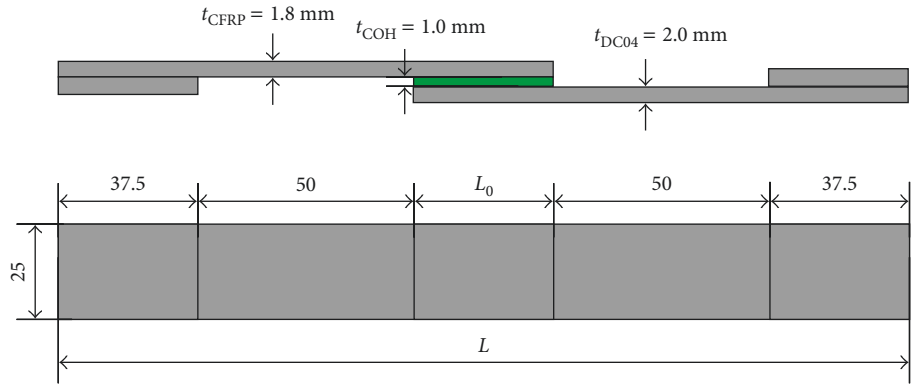

Figure 1: Schematic and dimensions of the single lap joints.

Table 4: Full-factorial experimental design with corresponding factors and levels.

Specimen	Adhesive type	L_0 (mm)	L (mm)
1	7779	12.5	187.5
2	7779	20	195
3	7779	30	205
4	7779	40	215
5	MA830	12.5	187.5
6	MA830	20	195
7	MA830	30	205
8	MA830	40	215

stress distribution and failure evolution analysis of the joints. The single lap joint tests were numerically built in a three-dimensional model with the geometry and boundary conditions exhibited in Figure 2(a). The end with CFRP substrate was fixed thoroughly to clamp, while another end with DC04 substrate could only move in the loading direction. The loading was terminated when the displacement reached the set value with regard to experimental loading cases.

The element type selected to mesh the adhesive was COH2D4, while the CFRP and DC04 adherends were meshed with C3H20. The mesh was refined to have more concentration of elements in both the adherends near the adhesive for further stress analysis. The properties for the adherends were mainly based on the results obtained in experiments (Tables 2 and 3).

To reproduce the behaviors of the adhesive, the bilinear traction separate law was used to simulate the elastic behavior up to a peak and subsequent degradation of material properties up to failure. During tensile testing, the damage occurs under mixed-mode loading (Model I, Model II, and Model III). Figure 2(b) shows the bilinear traction separate law under a single loading mode. The curve associates stress with displacements connecting homologous nodes of the cohesive elements. The initial linear elastic corresponds to the first section until the stress reaching the maximum, after the adhesive stiffness is degraded. The cohesive failure mainly contains two stages, including damage initiation and crack propagation. In the first stage, a quadratic nominal stress criterion is used to decide the damage initiation, as expressed below:

$$\left\{\frac{\langle\sigma_{\mathrm{I}}\rangle}{\sigma_{\mathrm{I}}^{0}}\right\}^{2}+\left\{\frac{\sigma_{\mathrm{II}}}{\sigma_{\mathrm{II}}^{0}}\right\}^{2}+\left\{\frac{\sigma_{\mathrm{III}}}{\sigma_{\mathrm{III}}^{0}}\right\}^{2}=1, \tag{1}$$

where σ_i and σ_i^0 (i = I, II, III) are the cohesion and interfacial strength under loading of Model I, Model II, and Model III, respectively. When the sum of the equation on the left is less than 1, there is no initial damage. Otherwise, initial damage will develop in the cohesive layer. B–K fracture criterion is applied to dominate the crack evolution in the second stage, as given below:

$$G_{\mathrm{IC}}+\left(G_{\mathrm{IIC}}-G_{\mathrm{IC}}\right)\left(\frac{G_{\mathrm{Shear}}}{G_{\mathrm{T}}}\right)^{\eta}=G_{\mathrm{C}}, \tag{2}$$

where G_{I}, G_{II}, and G_{III} represent fracture energy in three directions, respectively ($G_{\mathrm{Shear}} = G_{\mathrm{II}} + G_{\mathrm{III}}, G_{\mathrm{T}} = G_{\mathrm{I}} + G_{\mathrm{Shear}}$). $G_{i\mathrm{C}}$ (i = I, II, III) is the critical strain energy release rate under the respective models, and G_{C} is the total of the three. η is a constant that is related to the properties of the materials. When the left of the equation reaches the value of G_{C}, the initial crack begins to propagate and finally leads to adhesive failure.

In order to perform further failure evolution analysis, a parameter defined as scalar stiffness degradation (SDEG) is used to represent the degradation degree of the adhesive. This parameter can be any value between 0 and 1. When adhesive is in the initial elastic part of mixed-mode loading, the adhesive elements have no damage to any degree and SDEG is set equal to 0. While, the adhesive elements failure completely, SDEG is set equal to 1, and the element is deleted.

4. Results and Discussion

4.1. Mechanical Properties. The load-displacement curves for tensile testing are presented in Figure 3, including both

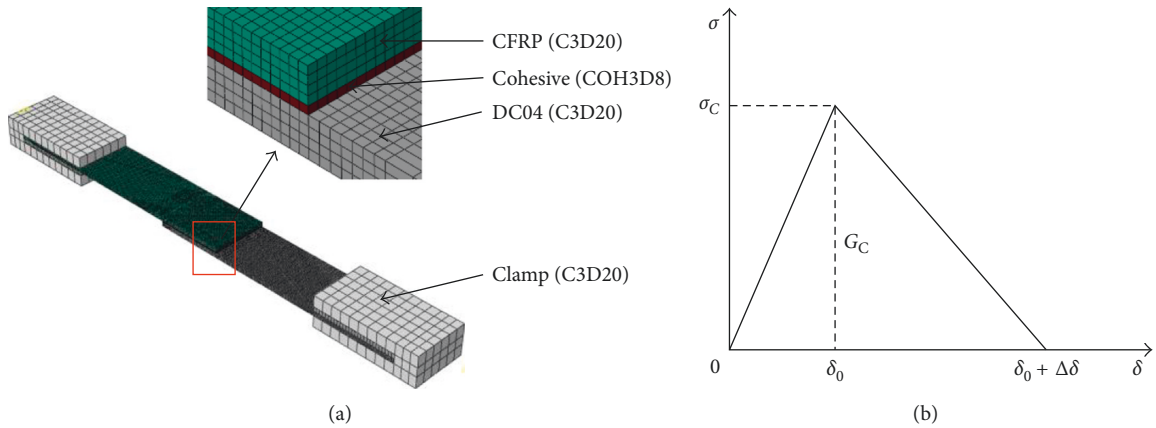

Figure 2: (a) The numerical model and (b) bilinear traction separate law for the finite element analysis.

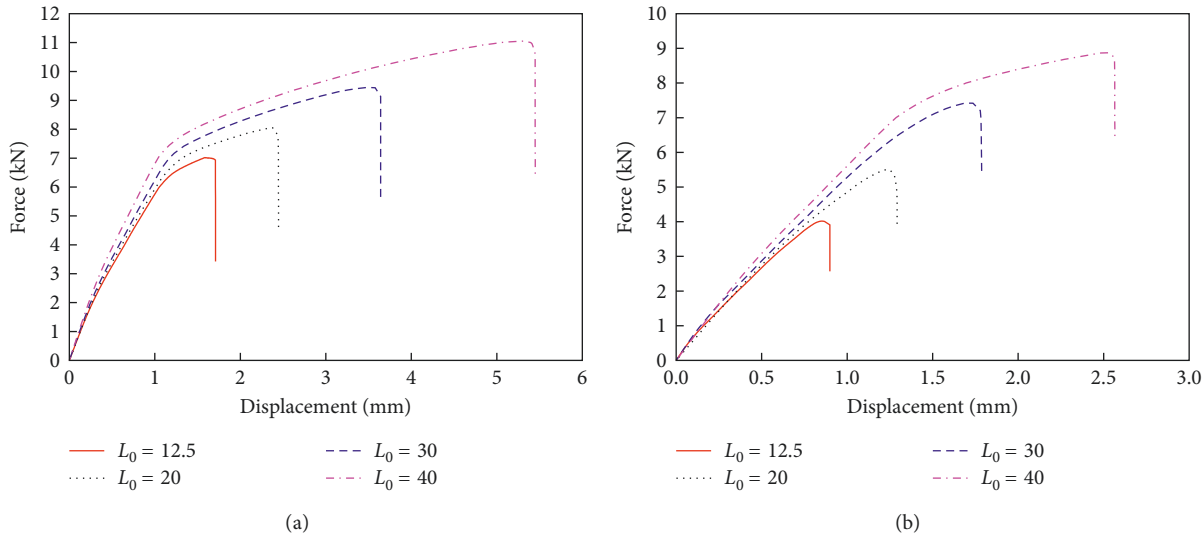

Figure 3: Tensile mechanical properties for joints using (a) 7779 structural adhesive and (b) MA830 structural adhesive.

adhesives with various overlap lengths. For joints using 7779 adhesive, the tensile process could be divided into three stages as shown in Figure 3(a). The slopes of the curves are kept constant in the first stage. When the load reached 2.5 kN, it entered the second stage, and the slope of the curves appeared a slight decrease. This mainly resulted from the strong toughness of the 7779 adhesive. As the adhesive was in force and began to soften, the stiffness of the joint decreased. When the load was between 6.5 and 7.5 kN in the third stage, the slope declined obviously, which was mainly due to that DC04 substrates achieved the yield strength, and plastic deformation occurs. As the loading continued, the joint finally failed when the load exceeded the strength. Since the failure load is the maximum force when the joint suffers failure, it is found that the failure load of the joint increased with the overlap length. For the joints using MA830 adhesive, the failure load also increased as overlap length increased, while the trend of the curves was different from those of using 7779 adhesive. When the overlap length was 12.5 and 20 mm, the slope of the curves was constant until complete failure of the joint. The maximum load was less than 6 kN, and thus there was no plastic deformation for the DC04 adherend. However, for the lap length of 30 and 40 mm, the maximum load was higher than 7 kN, and the slope of the curves appeared an obvious decrease. All the four curves showed no decrease when the load reaching 2.5 kN. This was mainly due to the fact that MA830 adhesive was more brittle, and there was no plastic deformation for MA830 adhesive.

4.2. Failure Load. For detailed analysis of the joint, Figure 4 summarizes the failure load and the normalized value. The error bars are also added. The deviation should be caused by deviation of experimental procedure and the dispersion of properties for the materials, especially the adhesive and the CFRP. Numerical results were found to agree well with the experimental results within 5% relative error. It was found that joints bonded with 7779 adhesive damaged at a higher load (2-3 kN) than that of the joints using MA830 adhesive with the same overlap length. This was mainly due to that the 7779 structural adhesive was much more ductile and

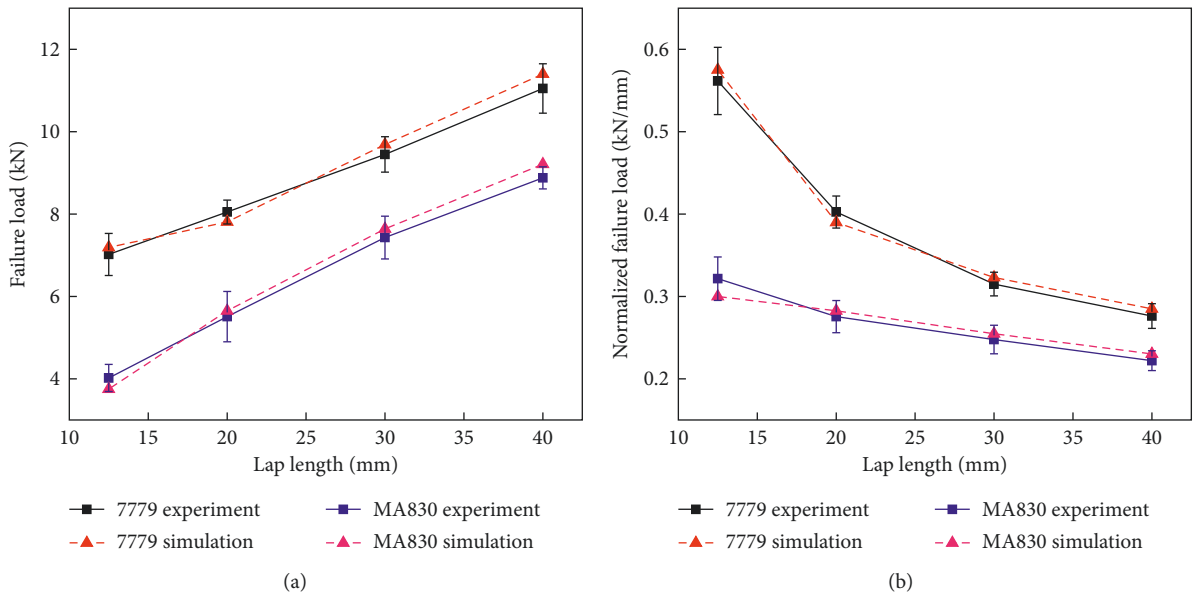

Figure 4: Experiment and simulation results: (a) failure load and (b) normalized failure load (failure load divided by overlap length).

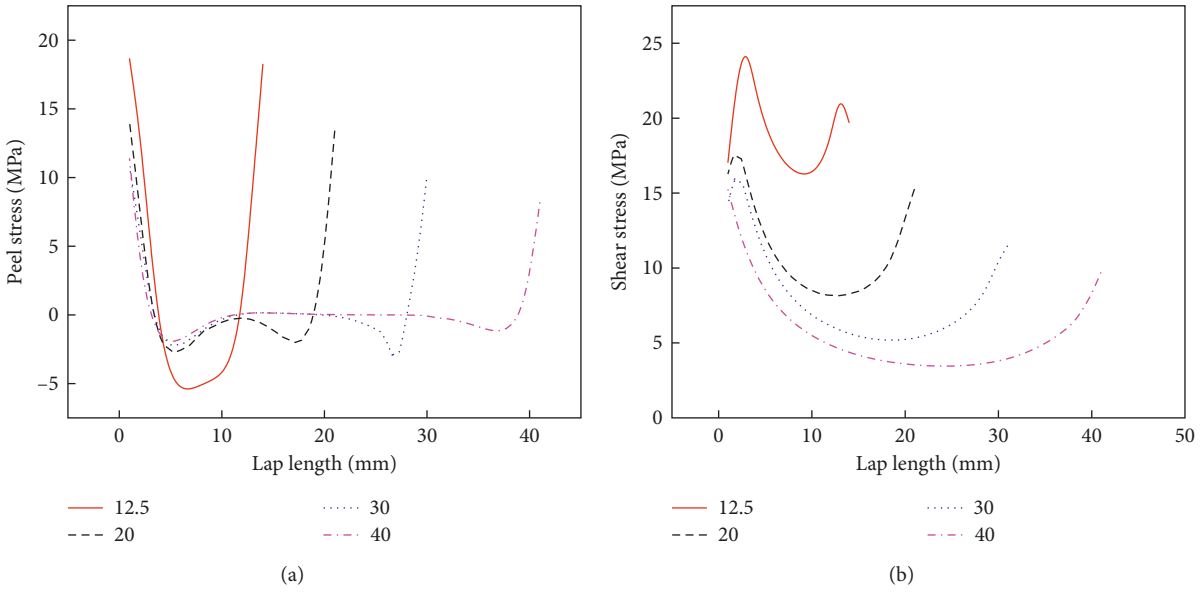

Figure 5: (a) Peel stress and (b) shear stress distributions with various overlap lengths.

flexible and could tolerate higher load than MA830 structural adhesive. For the failure load in Figure 4(a), both adhesives increased almost linearly with overlap length. As overlap length increased by 1 mm, the failure load of the 7779 structural adhesive joints increased by an average of about 147 N and that of the MA830 structural adhesive joint increased by an average of about 176 N. Moreover, normalized failure load, which is the failure load divided by the length of the overlap, is defined and plotted in Figure 4(b). The normalized failure load decreased dramatically with the increase of the overlap length which indicated that increasing the overlap length could strengthen the joint with only a limit degree.

4.3. Stress Distribution. The peel (S_{33}) and shear (S_{13}) stress distributions are compared at the adhesive layer in the middle width for various overlap lengths. All the stresses mentioned above were obtained under 6 kN load. Stress distributions in the adhesive layer of three typical moments during the whole tensile testing procedure were exhibited and compared with each other. Joints with MA830 adhesive were not considered in this section for the similar results.

The peel and shear stress distributions in the adhesive layer for different overlap lengths are presented in Figure 5. For the peel stress shown in Figure 5(a), the stress peaks located on the edge of the overlap region. And stress values on the left edge were slightly higher. This is mainly due to the

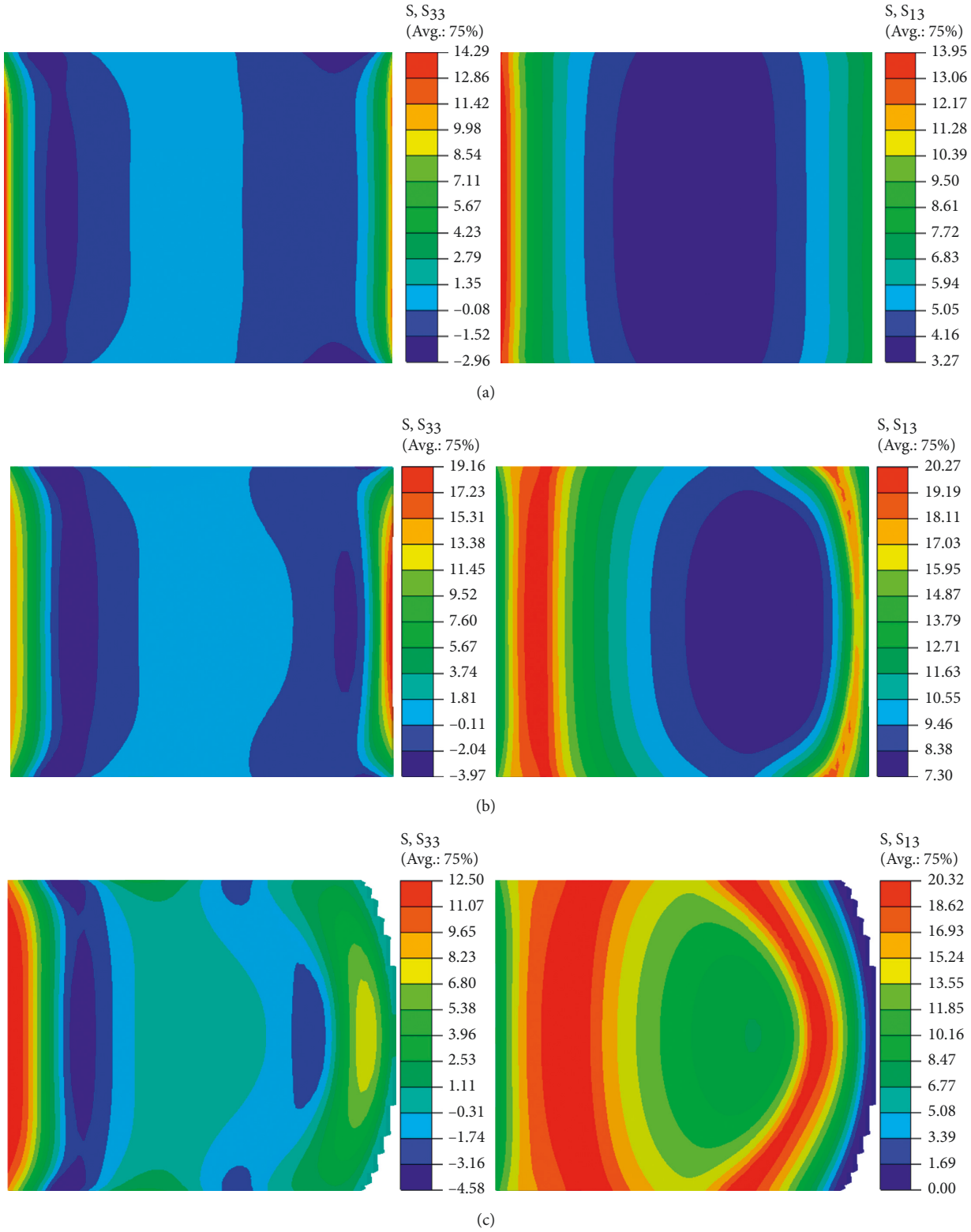

Figure 6: Peel and shear stress distributions at three different moments of the joint using 7779 adhesive with 30 mm overlap length. (a) $t = 6$ s; (b) $t = 49$ s; (c) $t = 110$ s.

two types of adherends with different stiffness. Thus, different degrees of adherend flexure appeared at the overlap edges. On the left overlap edge, the higher degree of flexure of the DC04 adherend produced higher peak peel stresses. As the overlap length increased, peel stress peaks decreased on both edges, and stress distributions were relatively much more uniform. For the shear stress exhibited in Figure 5(b), the maximum stress values on the left were 2–6 MPa higher

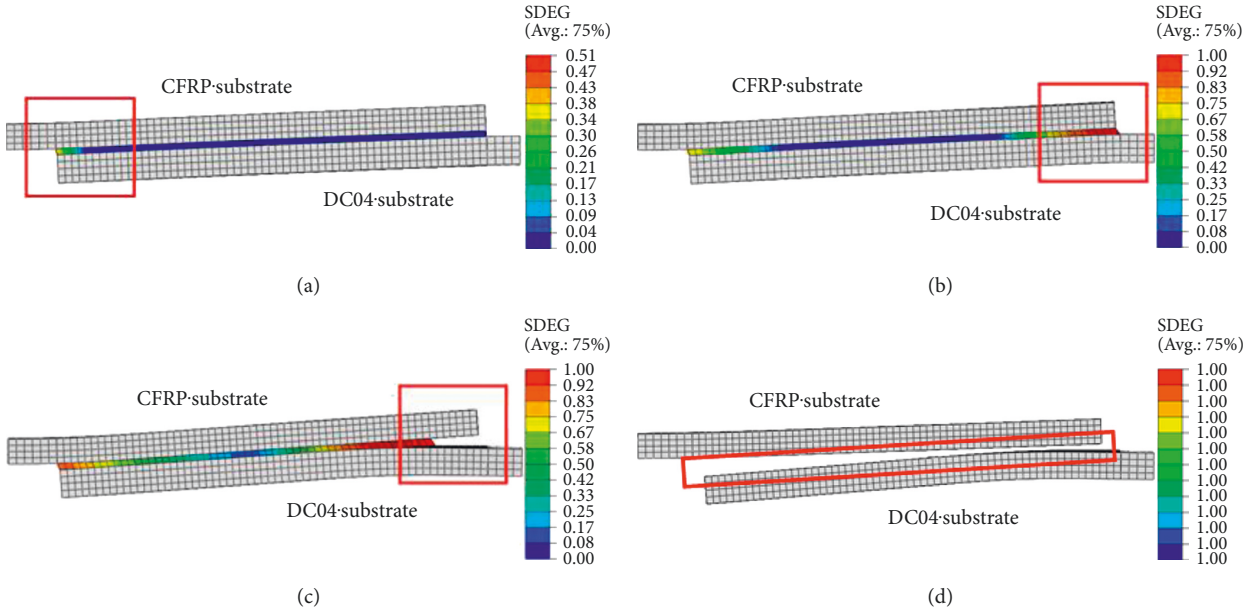

Figure 7: Failure process of the joints using 7779 adhesive with 30 mm overlap length: (a) beginning of degeneration; (b) degeneration proceeded; (c) cohesive failure appears and element deletion; (d) completely failure of adhesive layer.

than that on the right, which was mainly due to the fact that the two types of adherends had different tensile modulus. Furthermore, stress peaks of several types of joints located near the edge of the overlap rather than on the edge. As the overlap length increased, the position that peak stress appeared was close to both edges. This was mainly due to that under the 6 kN tensile loading, adhesive on both edges appeared degradation of varying degrees. This degeneration was slightly more severe on the left region. With increasing the overlap length, relatively more uniform peel distributions could be found. All the former analysis indicated that the increase of the lap length could reduce the stress concentration, thus leading to the failure load enhancement. However, both types of stress were distributed near the edges of the overlap region. The stresses in most of the middle regions were relatively small. The distribution characteristics indicated that increasing the overlap length can strengthen the joint with only a limit degree.

In order to investigate the stress distribution alongside the tensile loading process, different moments representing various stages were selected to analyze the stress state. The stress distributions are shown in Figure 6 with regard to three different moments, including $t = 6$ s, $t = 49$ s, and $t = 110$ s, referring to no plastic deformation of the DC04 substrate, large plastic deformation of the DC04 substrate, and approaching to the failure load, respectively. For the moment of $t = 6$ s, the tensile displacement was about 0.2 mm and in the stage of initial loading. The maximum peel stress of the adhesive was 14.92 MPa, and the maximum shear stress was about 13.95 MPa. While, the two stresses were far from their limits. For the moment of $t = 49$ s, the displacement approached to be 1.64 mm, which mainly resulted from the deformation of the CFRP since the CFRP produced larger deformation than that of the DC04 adherend. The effect of asymmetric rigidity of the adherends could be seen in stress distribution for its inhomogeneous distributions of both shear and peel stresses. On the right side of the adhesive layer, the shear stress dropped dramatically; however, the decline trend on the left was much slower. This was mainly due to that DC04 adherend produced a plastic deformation at this moment so that the tensile force was not transmitted to the adhesive on the right. The maximum peel stress reached 19.16 MPa, which was far from the stress limit (29.43 MPa). However, the highest shear stress was about 20.27 MPa and approached shear stress limits (20.4 MPa). When time is $t = 110$ s, some of the cohesive elements became invalid and were deleted, which meant that complete failure appeared in the adhesive layer. The whole joint assumed to be almost the maximum load at this moment. The peel stress was 12.55 MPa, still far from reaching the limit stress. The maximum shear stress was 20.32 MPa and was very close to the stress limit, which implied that the cause of the joint failure was that the shear stress reached the shear limit of the adhesive.

4.4. Failure Propagation. Joint using 7779 structural adhesive with 30 mm overlap length was selected for the failure propagation analysis. As described in Section 3, SDEG is a parameter that represents the degradation degree of the adhesive. Figure 7(a) shows that the adhesive on the left was first degenerated. This was related to the relatively higher peel and shear stresses which was analyzed in Section 4.2. As the tensile loading continued, adhesive on the right shown in the Figure 7(b) also began to degenerate and the degeneration was much more severe than that on the left. Furthermore, SDEG of adhesive on the right firstly reached the value of 1, and the failure elements were deleted as could be seen in Figure 7(c). This phenomenon was mainly due to that two different materials were used as the adherends. Adhesive was fixed to the two substrates with

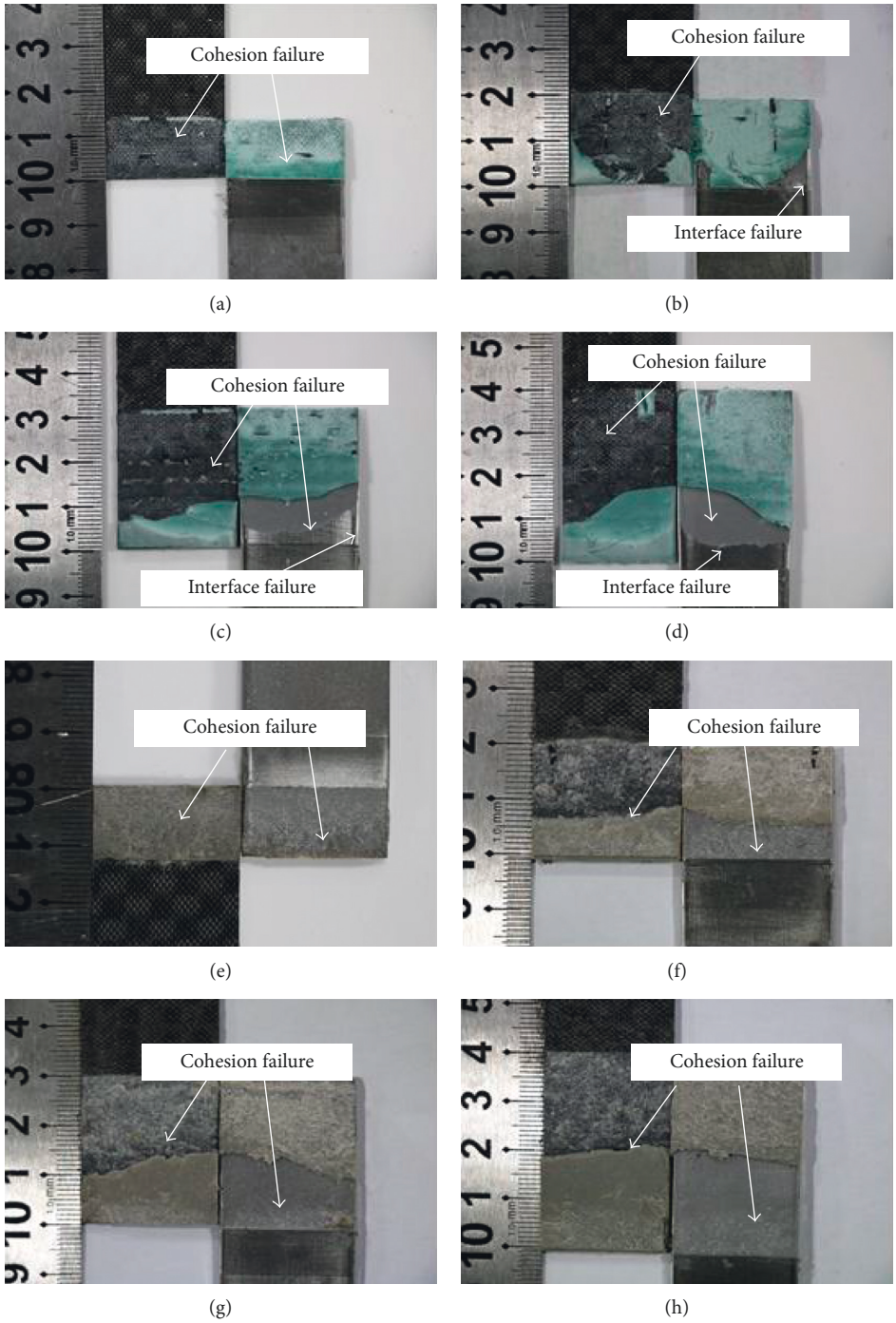

Figure 8: Failure models of 7779 adhesive joints with overlap lengths of (a) 12.5 mm, (b) 20 mm, (c) 30 mm, and (d) 40 mm. Failure models of MA830 adhesive joints with overlap lengths of (e) 12.5 mm, (f) 20 mm, (g) 30 mm, and (h) 40 mm.

various stiffness. For a specific loading, CFRP produced a larger deformation than the DC04 adherend. Thus, adhesive on the right edge deformed much more severe, and failure appeared in this region at the early stage. In Figure 7 (d), all the adhesive elements were in failure and deleted, and the DC04 adherends produced permanent plastic deformations in the joint area. The asymmetry degeneration of the adhesive layer could be easily seen from the failure process and this asymmetry distribution mainly resulted from the two different adherends.

4.5. Failure Modes. The failure modes of the two adhesives with various overlap lengths are shown in Figure 8. For the 7779 structural adhesive, there were two main failure modes including cohesion failure and interface failure. When the overlap length was 12.5 mm, it merely presented cohesion failure as shown in Figure 8(a). As the overlap length increased, the bending moment caused by load eccentricity became more severe. The peel stress on the edge of the overlap produced higher values and reached the peel stress limit of the adhesive. Thus, interface failure occurred and

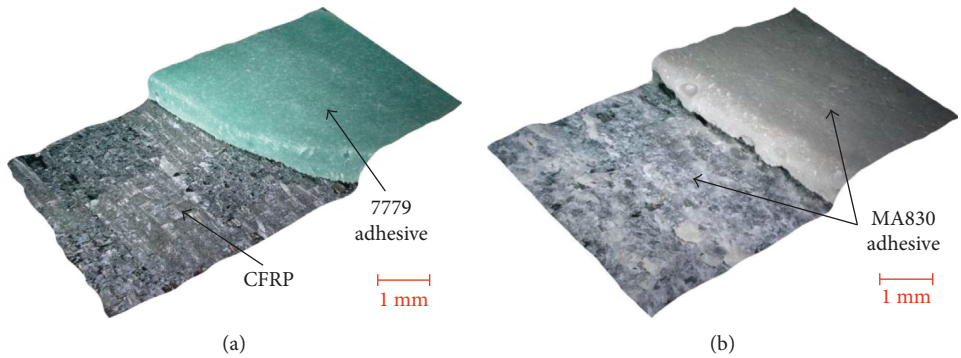

Figure 9: The morphology of the facture surfaces confirms the (a) interface failure and (b) cohesion failure (observed through a digital microscope KEYENCE VHX-5000).

became one of the failure modes as seen in Figure 8. Furthermore, the failure of bonding interface only occurred on the bonding surface between adhesive layer and DC04 substrate. This indicated that the 7779 adhesive had a better connection with CFRP adherends than DC04 adherends. As for joints of MA830 structural adhesive as shown in Figure 8, there was only cohesion failure for all different overlap lengths. This is mainly owing to the fact that joints of MA830 adhesive fail at a relative low load. Thus, peel stresses on the edge of the overlap were far from the stress limit of the adhesive, and there was no interface failure.

The detailed observations of the morphology for the facture surfaces were conducted through a digital microscope (KEYENCE VHX-5000). The morphologies of the facture surfaces are presented in Figure 9. As shown in Figure 9(a), for the 7779 adhesive in the joint, the adhesive is completely peeled off from the CFRP, and the CFRP is obviously visible in this specimen. Thus, this observation firmly confirms the interface failure model. On the contrary, as shown in Figure 9(b), residual MA830 adhesive can be clearly found on the CFRP, demonstrating the cohesion failure occurred within the adhesive.

5. Conclusions

The present work investigated the influences of the adhesive type and overlap length on the mechanical behavior and failure modes of bonded single lap joints via experimental and numerical studies. Main conclusions can be drawn as follows:

(1) The joint strength was found to be highly dependent on adhesive type and overlap length. Joints using 7779 structural adhesive provided 2-3 kN failure load higher than that using MA830 structural adhesive. And failure load with two adhesives increased about 147~176 N with increasing 1 mm of the overlap length.

(2) A finite element analysis model was established, and numerical results were within 5% relative error on predicting the failure load and joint strength compared with the experimental results. There was severe stress concentration on the edge of the joint. And the stress distributions in the overlap area were nonuniform. The peel stress was responsible for the interface failure, and the cohesion failure is mainly caused by large shear stress. The shear stress reaching the limit stress of the adhesive was the main reason for the failure of the adhesive layer.

(3) An asymmetry degeneration of the adhesive layer could be easily seen from the failure process analysis, which was mainly due to the asymmetric rigidity of the adherends.

(4) The type of the adhesive and level of overlap length affected the failure modes significantly. The failure modes of the joints of 7779 structural adhesive presented cohesion failure and interface failure. While, MA830 adhesively bonded joints merely showed interface failure irrespective of the overlap length.

Conflicts of Interest

The authors declare that they have no conflicts of interest.

Acknowledgments

The authors are grateful for the support by the National Natural Science Foundation of China under Grant nos. 11602081 and 11302063. This work is also supported by Natural Science Foundation of Hunan Province under Grant no. 2017JJ3031, and the Fundamental Research Funds for the Central Universities under Grant no. 531107040934.

References

[1] K. J. Jadee and A. R. Othman, "Fiber reinforced composite structure with bolted joint—a review," *Key Engineering Materials*, vol. 471-472, pp. 939–944, 2011.

[2] D. V. T. G. Pavan Kumar, S. Sathiya Naarayan, S. Kalyana Sundaram, and S. Chandra, "Further numerical and experimental failure studies on single and multi-row riveted lap joints," *Engineering Failure Analysis*, vol. 20, pp. 9–24, 2012.

[3] A. T. T. Nguyen, C. K. Amarasinghe, M. Brandt, S. Feih, and A. C. Orifici, "Loading, support and geometry effects for pin-reinforced hybrid metal-composite joints," *Composites Part A: Applied Science and Manufacturing*, vol. 98, pp. 192–206, 2017.

[4] N. Chowdhury, W. K. Chiu, J. Wang, and P. Chang, "Static and fatigue testing thin riveted, bonded and hybrid carbon fiber double lap joints used in aircraft structures," *Composite Structures*, vol. 121, pp. 315–323, 2015.

[5] A. Riccio, R. Ricchiuto, F. Di Caprio, A. Sellitto, and A. Raimondo, "Numerical investigation of constitutive material models on bonded joints in scarf repaired composite laminates," *Engineering Fracture Mechanics*, vol. 173, pp. 91–106, 2017.

[6] G. R. Rajkumar, M. Krishna, H. N. Narasimhamurthy, and Y. C. Keshavamurthy, "Statistical investigation of the effect of process parameters on the shear strength of metal adhesive joints," *Journal of The Institution of Engineers (India): Series C*, vol. 98, pp. 335–342, 2016.

[7] L. Liao, C. Huang, and T. Sawa, "Effect of adhesive thickness, adhesive type and scarf angle on the mechanical properties of scarf adhesive joints," *International Journal of Solids and Structures*, vol. 50, no. 25-26, pp. 4333–4340, 2013.

[8] A. J. Gunnion and I. Herszberg, "Parametric study of scarf joints in composite structures," *Composite Structures*, vol. 75, no. 1–4, pp. 364–376, 2006.

[9] L. F. M. da Silva, T. N. S. S. Rodrigues, M. A. V. Figueiredo, M. F. S. F de Moura, and J. A. G. Chousal, "Effect of adhesive type and thickness on the lap shear strength," *Journal of Adhesion*, vol. 82, no. 11, pp. 1091–1115, 2006.

[10] D.-B. Lee, T. Ikeda, N. Miyazaki, and N.-S. Choi, "Effect of bond thickness on the fracture toughness of adhesive joints," *Journal of Engineering Materials and Technology*, vol. 126, no. 1, p. 14, 2004.

[11] M. You, Z. Li, X.-L. Zheng, S. Yu, G.-Y. Li, and D.-X. Sun, "A numerical and experimental study of preformed angle in the lap zone on adhesively bonded steel single lap joint," *International Journal of Adhesion and Adhesives*, vol. 29, no. 3, pp. 280–285, 2009.

[12] S. L. S. Nunes, R. D. S. G. Campilho, F. J. G. Da Silva et al., "Comparative failure assessment of single and double lap joints with varying adhesive systems," *Journal of Adhesion*, vol. 92, no. 7–9, pp. 610–634, 2016.

[13] M. You, Z.-M. Yan, X.-L. Zheng, H.-Z. Yu, and Z. Li, "A numerical and experimental study of adhesively bonded aluminium single lap joints with an inner chamfer on the adherends," *International Journal of Adhesion and Adhesives*, vol. 28, no. 1-2, pp. 71–76, 2008.

[14] S. Akpinar, M. O. Doru, A. Özel, M. D. Aydin, and H. G. Jahanpasand, "The effect of the spew fillet on an adhesively bonded single-lap joint subjected to bending moment," *Composites Part B: Engineering*, vol. 55, pp. 55–64, 2013.

[15] A. M. Pereira, J. M. Ferreira, F. V. Antunes, and P. J. Bártolo, "Analysis of manufacturing parameters on the shear strength of aluminium adhesive single-lap joints," *Journal of Materials Processing Technology*, vol. 210, no. 4, pp. 610–617, 2010.

[16] C. Sperandio, J. Bardon, A. Laachachi, H. Aubriet, and D. Ruch, "Influence of plasma surface treatment on bond strength behaviour of an adhesively bonded aluminium-epoxy system," *International Journal of Adhesion and Adhesives*, vol. 30, no. 8, pp. 720–728, 2010.

[17] M. Elhannani, K. Madani, E. Legrand, S. Touzain, and X. Feaugas, "Numerical analysis of the effect of the presence, number and shape of bonding defect on the shear stresses distribution in an adhesive layer for the single-lap bonded joint; part 1," *Aerospace Science and Technology*, vol. 62, pp. 122–135, 2017.

[18] A. Riccio, G. Di Felice, F. Scaramuzzino, and A. Sellitto, "A practical tool for the preliminary design of bonded composite repairs," *Applied Composite Materials*, vol. 21, no. 3, pp. 495–509, 2014.

[19] K. N. Anyfantis and N. G. Tsouvalis, "Loading and fracture response of CFRP-to-steel adhesively bonded joints with thick adherents—part II: numerical simulation," *Composite Structures*, vol. 96, pp. 858–868, 2013.

[20] T. E. A. Ribeiro, R. D. S. G. Campilho, L. F. M. da Silva, and L. Goglio, "Damage analysis of composite–aluminium adhesively-bonded single-lap joints," *Composite Structures*, vol. 136, pp. 25–33, 2016.

[21] A. Riccio, A. Sellitto, S. Saputo, A. Russo, M. Zarrelli, and V. Lopresto, "Modelling the damage evolution in notched omega stiffened composite panels under compression," *Composites Part B: Engineering*, vol. 126, pp. 60–71, 2017.

[22] W. Xu and Y. Wei, "Strength and interface failure mechanism of adhesive joints," *International Journal of Adhesion and Adhesives*, vol. 34, pp. 80–92, 2012.